Identifying the Process Shift with Robust Control Charts in the Presence of Contamination

Chiong Liong Wong[1], *Kooi Huat* Ng[1], and *Wei Lun* Tan[1]

[1]Department of Mathematical and Actuarial Sciences, Lee Kong Chian Faculty of Engineering and Science, Universiti Tunku Abdul Rahman, Jalan Sungai Long, Bandar Sungai Long, Cheras, 43000 Kajang, Selangor, Malaysia

Abstract. Conventional control charts have traditionally been reliable tools for monitoring processes under the assumption of normally distributed data. However, real-world data often deviate from this idealized normality, leading to reduced charting performance and potentially causing process anomalies to go unnoticed. In this study, by integrating robust statistical estimators and innovative charting techniques, robust control charts demonstrate their capability to effectively detect process shifts and abnormalities in a variety of challenging settings. Through Monte Carlo simulation studies and a real dataset application, this research provides insights into the benefits and limitations of robust control charts. Our findings indicate that the proposed robust control charts show a notable performance in detecting data anomalies, specifically for the shift in mean, outperforming conventional charts in this regard. Comparison among the three robust location estimators via simulations, namely Huber (*H*) and Biweight (*B*) estimators as well as the proposed Biweight estimator integrating the *M-Scale* (*BM*) estimator also demonstrate its superiority in handling shifting in mean process situations.

1 Introduction

Control charts are widely used in statistical process control analysis as a primary tool for monitoring processes and detecting variations ([1]). The main objective of control charts is to determine whether a process is in control or beyond control. These charts have applications across diverse fields apart from the commonly applied field in manufacturing, such as finance ([2]), healthcare ([3]), etc. Conventional control charts, such as Shewhart *X-bar* (with *S* or *R*) chart, *R* chart and Moving Range chart have long been established and commonly used for this purpose. However, conventional control charts have their inherent limitations when dealing with contamination and non-normal datasets. If the underlying data distribution deviates from normality, the accuracy of the estimators diminishes, rendering the control chart ineffective in detecting process changes and potential outliers ([4]). In reality, many real-world datasets exhibit non-normal characteristics, making the assumption of a normal distribution impractical. To tackle these challenges, statisticians have developed several robust control charts since the 1970s, presenting them as valuable tools for ensuring process stability and identifying deviations, particularly in scenarios involving non-normality, outliers, and other data anomalies. An early development in the history of robust estimates

of location was introduced by Andrews et al.[5] in 1972. Iglewicz and Hoaglin [6] constituted a strong study on how to detect and handle outliers. In 1996, an article was published by Sullivan et al.[7] that has been subject of much discussion on a control chart for preliminary analysis of individual observations. They investigated the benefits of employing the *X* control chart and moving range control chart that includes the ability to identify multiple shifts and discern whether an out-of-control signal is primarily attributed to a change in the mean, variance, or a combination of both. Lax [8] presented the results of a Monte Carlo study of the robustness of scale estimates in the presence of long-tailed, symmetric distributions. The comparison seems to demonstrate that the most successful *A*-estimator uses the Biweight weighting function, which is also the basis for high-performance robust location estimates. Tatum [9] and Huber [10] proposed improved methods of scale on skewed data which are able to achieve higher efficiency compared to other estimators.

Seminal work on in-control robustness comparison of different control charts was carried out by Abid et al. [11]. It is observed that the Mixed EWMA-CUSUM (*MEC*) scheme demonstrates strong in-control robustness performance across normal, non-normal, and contaminated normal distributions when compared with competing schemes. There are various robust methods to deal with the contaminations such as Median Absolute Deviation (*MAD*), *M*-estimations, redescending *M*-estimations, etc. To this end, Abu-Shawiesh et al [12] provided extensive discussions of the application of simple robust control chart based on *MAD* while Ariza Guerrero et al. [13] proposed a framework for the application of robust multivariate control chart with Winsorized mean.

This study aims to assess the efficacy of our proposed method within the framework of existing robust methods and our innovation. We propose to apply *M-Scale* estimation which was first introduced by Yohai [14] based on the procedures offered by De Mast and Roes [15] to examine its robustness from our proposed method. It is crucial to emphasize that the techniques outlined in this paper are designed for retrospective analysis. In simpler terms, the proposed method is not intended for identifying deviations in a live process but rather for drawing conclusions based on a dataset from the past. The performance between the existing robust methods and our proposed method will also be investigated via extensive simulations.

2 Review of the existing shewhart control chart for individual measurements

The individual control chart is a common statistical control chart employed in quality control and process monitoring with the purpose of monitoring the stability and consistency of a process over time, particularly when dealing with variables data. Unlike charts based on subgroup averages, the individual control chart relies on the distribution of individual measurements. This design is advantageous for processes where it might be inconvenient to collect multiple measurements simultaneously. The control limits incorporating with Average Moving Range (*AMR*) are

$$UCL = \hat{\mu} + 3\frac{\overline{MR}}{d_2}, \tag{1a}$$

$$LCL = \hat{\mu} - 3\frac{\overline{MR}}{d_2} \tag{1b}$$

$\hat{\mu}$ is the overall mean in the sample while d_2 is the statistical constant 1.128 and $\overline{MR}$ is

$$\overline{MR} = \frac{1}{n-1}\sum_{i=1}^{n-1}|y_i - y_{i+1}| \tag{2}$$

Here, y_i and y_{i+1} are individual data points or measurements in a sequence. Occurrences of points outside the control limits or displaying unusual patterns may indicate the existence of special causes of variation, suggesting the necessity for additional investigation.

3 Methodology

3.1 The proposed control charting procedure

In this paper, the focus is narrowed down to the exploratory process, specifically phase I analysis. We concentrate solely on data that exhibits a change point in the mean while maintaining an unaltered variance. It is worth noting that the change point itself, as well as the population mean and standard deviation before and after the change point, remain unknown. To address these circumstances, we implement the charting procedures proposed by De Mast and Roes [15] as below:

1. First, detect the change points and test the significance of these change points. Subsequently, segment the original dataset into intervals corresponding to these shifts.
2. Compute the means of the intervals between successive shifts (by using the proposed robust estimators). The process standard deviation is then estimated following the computation of these robust estimators.
3. Finally, on the basis of the derived estimations, establish upper and lower control limits for each interval. Any data points that fall beyond these control limits are deemed as outliers.

Peihua [16] and Sheikhrabori & Aminnayeri [17] applied Maximum Likelihood Estimation method for estimating the change point in process mean, the population mean and standard deviation. For an in-control process, all random variables y_i are assumed to be drawn from the same normal distribution

$$y_i = \mu + \varepsilon_i, \qquad i = 1, \dots, n, \tag{3}$$

with ε_i i.i.d. $N(0, \sigma^2)$, where μ is the overall process mean of the data. In the event of the occurrence of a single shift, the model is demonstrated as

$$\begin{cases} y_i = \mu_1 + \varepsilon_i, & i = 1, \dots, \tau \\ y_i = \mu_2 + \varepsilon_i, & i = \tau + 1, \dots, n \end{cases} \tag{4}$$

with ε_i i.i.d. $N(0, \sigma^2)$. In which case, $\{y_1, y_2, \dots, y_\tau\}$ is normally distributed with $N(\mu_1, \sigma^2)$ and $\{y_{\tau+1}, y_{\tau+2}, \dots, y_n\}$ having the normal distribution $N(\mu_2, \sigma^2)$, where $\mu_1 \neq \mu_2$ with different constant values, the random variables $\{y_1, y_2, \dots, y_n\}$ have a change point in its mean at τ. Here, μ_1 represents the population mean before the shift, while μ_2 denotes the population mean of data after the shift. In this scenario, we can employ the log-likelihood function defined as

$$l(\mu_1, \mu_2, \sigma, \tau) = \frac{n}{2}\log(2\pi\sigma^2) + \frac{1}{2\sigma^2}\sum_{i=1}^{\tau}(y_i - \mu_1)^2 + \sum_{i=\tau+1}^{n}(y_i - \mu_2)^2. \tag{5}$$

Our objective is to estimate the parameters by minimizing the likelihood function to obtain the maximum likelihood estimates (MLEs) and is usually denoted as *M*-estimates. *M*-estimates of the targeted parameters, i.e., $\mu_1, \mu_2, \sigma, \tau$ in the function are the solution of the Eq. (6) as shown below

$$(\hat{\mu}_1, \hat{\mu}_2, \hat{\sigma}, \hat{\tau}) = \arg\min_{\mu_1,\mu_2,\sigma,\tau} l(\mu_1, \mu_2, \sigma, \tau). \tag{6}$$

Conventionally, sample mean is adopted in estimating the population mean, μ, due to its unbiased nature. However, in real-world applications, this estimation can be heavily influenced by outliers since it incorporates all measurements in its calculation. This can result in an unrepresentative estimate in the presence of outliers. To obtain a robust estimates of location parameters μ_1 and μ_2 against the possible anomalies, we employ redescending ψ function suggested by Maronna et al. [18] to calculate the *M*-estimates. This function calculates the *M*-estimation of the parameters effectively and reduces the influence of extreme values y_i while maintaining the estimation efficiency within the underlying distribution.

There are several methods to compute the *M*-estimates, such as Newton-Raphson, iterative pseudo-observations, and iterative reweighting algorithm. Among these methods, the iterative reweighting algorithm is applied. $\hat{\mu}_1$ and $\hat{\mu}_2$ are now the solutions of

$$\sum_{i=1}^{\tau} \psi\left(\frac{y_i - \hat{\mu}_1}{cs_0}\right) = 0, \tag{7a}$$

$$\sum_{i=\tau+1}^{n} \psi\left(\frac{y_i - \hat{\mu}_2}{cs_0}\right) = 0 \tag{7b}$$

where

$$s_0 = median\{|y_i - m|\}_{i=1,\dots n,} \tag{8}$$

with $m = m_1$ if $1 \le i \le \tau$, and $m = m_2$ if $\tau + 1 \le i \le n$, where m_1 and m_2 are the median of $y_1, \dots, y_\tau$ and $y_{\tau+1}, \dots, y_n$ respectively. The recommended value of c is set as 9 validated from a series of simulations. Once the process mean estimate is determined, the final process standard error estimate is computed by

$$\hat{\sigma} = \frac{\sqrt{n} c s_0 \left(\sum_{i=1}^{\tau} \psi^2\left(\frac{y_i - \hat{\mu}_1}{cs_0}\right) + \sum_{i=\tau+1}^{n} \psi^2\left(\frac{y_i - \hat{\mu}_2}{cs_0}\right)\right)^{\frac{1}{2}}}{\left|\sum_{i=1}^{\tau} \psi'\left(\frac{y_i - \hat{\mu}_1}{cs_0}\right) + \sum_{i=\tau+1}^{n} \psi'\left(\frac{y_i - \hat{\mu}_2}{cs_0}\right)\right|} \tag{9}$$

with ψ' refers to the derivative of ψ, where ψ itself is the derivative of ρ. Walach et al. [19] explored various options for the ψ function in outlier detection, including choices such as Huber's and Tukey's Biweight ψ functions. These ψ functions were introduced for their ability to resist outliers and handle deviations from normality. Among these alternatives, we have chosen the Tukey's Biweight function, which is more commonly utilized and demonstrated slightly superior performance compared to Huber's function, as indicated by the simulation results presented in Table 1. The Tukey's Biweight function is defined as follows:

$$\psi(u) = \begin{cases} u(1-u^2)^2, |u| \le 1 \\ 0 \qquad\quad , |u| > 1 \end{cases}. \tag{10}$$

The change point is then determined via the solution of

$$\hat{\tau} = \arg\min_{2 \le \tau \le n-2} l(\hat{\mu}_1, \hat{\mu}_2, \hat{\sigma}, \tau), \tag{11}$$

Although *MAD* is a reliable scale estimator for heavily skewed data (Adekeye et al., [20]) since it possesses high breakdown-point of 50%, the original standard error s_0 of the estimator in Eq. (9) which is initially determined by Median Absolute Deviation (*MAD*) is less efficient compared to the standard deviation which is an unbiased scale estimator when data is normally distributed (Abu-Shawiesh, [21]). To address this limitation and maintain a level of generality that *MAD* cannot achieve, we propose employing *M*-Estimate of Scale, denoted as *M-Scale* (S_M) which offers a unique combination of a similar breakdown point as *MAD* and higher efficiency at normal distribution with the presence of contamination. In doing so, we anticipate superior performance in detecting the shift in mean amid contamination by incorporating the *M-Scale* compared to other forms of robust estimators. The computed *M-Scale* estimator will be integrated into the evaluation of $\hat{\mu}_1$ and $\hat{\mu}_2$ and $\hat{\sigma}$ as outlined in Eq. (7) and Eq. (9), by substituting the initial standard scale estimate s_0 with the *M-Scale* estimate.

With properties that ρ function is bounded, even, continuous, and non-increasing, the *M-Scale* (S_M), is derived as the solution of

$$\frac{1}{n}\sum_{i=1}^{n}\rho(u) = \frac{1}{n}\sum_{i=1}^{n}\rho\left(\frac{r_i}{S_M}\right) = \delta \tag{12}$$

where u represents $\frac{r_i}{S_M}$, $r_i = y_i - \mu_0$ represents the residual, and δ is defined to be $E_{\emptyset}(\rho(r)) = \delta$, in which $\emptyset$ represents the standard normal distribution. To illustrate further, the detailed steps for numerical algorithm of the *M-Scale* estimate are as follows:

1. Initiate the calculation by estimating the initial scale, denoted as S_{M_0}, using the normalized median absolute deviation (*MADN*).
2. For $k = 0, 1, 2, \ldots$, compute the weight function of S_{M_k}, then based on this weight function, calculate the next *M-Scale* estimate $S_{M_{k+1}}$ as given in Eq. (15)

$$w_{k,i} = W\left(\frac{r_i}{S_{M_k}}\right), \qquad 1 \le i \le n \tag{13}$$

where the weight function is defined as

$$W(t) = \begin{cases} \dfrac{\rho(t)}{t^2}, & if\ t \neq 0 \\ \rho''(0), & if\ t = 0 \end{cases}, \tag{14}$$

and

$$S_{M_{k+1}} = \sqrt{\frac{1}{n\delta}\sum_{i=1}^{n} w_{k,i} \times r_i^2}\,. \tag{15}$$

3. Continue to iterate step 2 until

$$\left|\frac{S_{M_{k+1}}}{S_{M_k}} - 1\right| < 10^{-6}. \tag{16}$$

Here, μ_0 is the initial location estimator, the median of y_i for $1 \le i \le n$. The final estimate of S_M is given by the converged value of S_{M_k}.

3.2 Control limits

Upon the computation of $\hat{\mu}_j$ and $\hat{\sigma}$ as described in the previous section, the chart control limits are determined via

$$UCL_j = \hat{\mu}_j + h\sqrt{\frac{\hat{\tau}_{j+1}-\hat{\tau}_j-1}{\hat{\tau}_{j+1}-\hat{\tau}_j}} \cdot \hat{\sigma} \tag{17a}$$

$$LCL_j = \hat{\mu}_j - h\sqrt{\frac{\hat{\tau}_{j+1}-\hat{\tau}_j-1}{\hat{\tau}_{j+1}-\hat{\tau}_j}} \cdot \hat{\sigma} \tag{17b}$$

where $\hat{\tau}_1 = 0$ and $\hat{\tau}_{k+1} = n$. De Mast and Roes [15] adopted the conventional value $h = 3$ while $\sqrt{\frac{\hat{\tau}_{j+1}-\hat{\tau}_j-1}{\hat{\tau}_{j+1}-\hat{\tau}_j}}$ served as the factor that characterizes the relationship between y_i and the control limits.

4 Result and discussion

4.1 Empirical study

As an illustrative example, a real dataset spanned from 2018 to 2021 is excerpted from the concentration of particulate matter, i.e. PM_{10}. As an indicator of air pollution, we proposed to monitor the flow of vehicles on the road through the PM_{10} index. Our study centered on Petaling Jaya area, which is one of the busiest towns in Malaysia with the highest vehicular flow, located in the state of Selangor. Since our dataset ranges from 2018 to 2021, the individual control chart is appropriate for analyzing the sequential, time-ordered nature of the data rather than focusing on the mean of subgroup measurements. It allows us to monitor how each individual measurement deviates from its expected value over time. The individual control chart is more adept at capturing gradual changes and trends in individual data points. This is important in our study to expect a gradual decrease in PM_{10} concentration due to the Covid-19 pandemic and the associated reduction in vehicular flow.

From inspection, both individual control chart and the proposed robust control chart reveal the presence of assignable causes. It is at first natural to expect that a control chart for the above given data would signal the shifts in mean at $i = 28$ and $i = 35$, with the remaining variation being attributed to white noise. However, due to the distortion of the constructed control limit for individual control chart possibly by some outlying values as displayed in Fig. 1, we can observe that there are three signals that located outside the control limits indicating the first shift which is detected at $i = 28$.

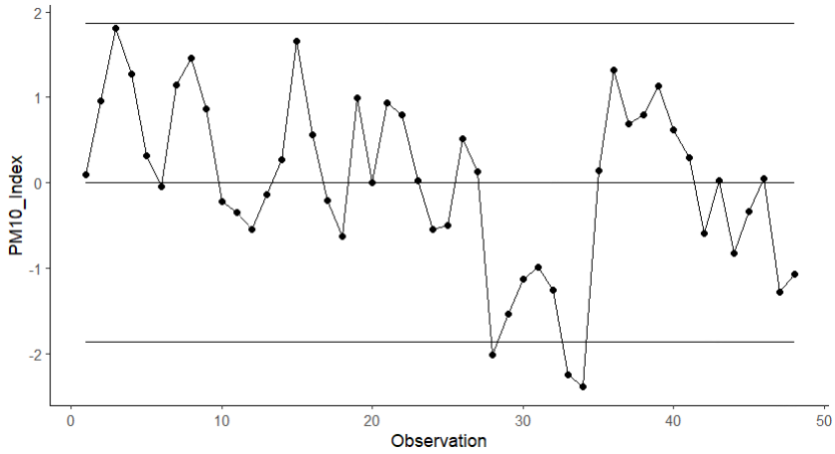

Fig. 1. Individual Control Chart on PM_{10} Index.

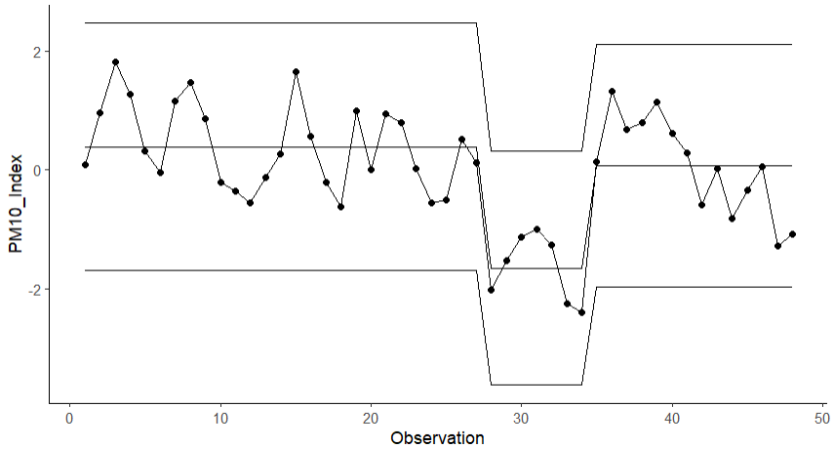

Fig. 2. Proposed Robust Individual Control Chart on PM_{10} Index.

The index of PM_{10} values observed through the proposed robust individual control chart integrating the proposed change point detection approach (utilizing the *M-Scale* estimator) successfully identified the expected changes. The first change was observed in March 2020 (28th observation), likely attributed to the implementation of the Movement Control Order (MCO), which resulted in the reduced vehicles usage. While the second change was detected in December 2021 (35th observation), which seems to indicate that the change in estimated mean for PM_{10} increases after the 35th observation, possibly due to less stringent MCO measures aimed at curbing the spread of the Covid-19 pandemic causing the traffic flow to increase. The nature of the detected change suggests that, after the 35th observation, there is a noticeable increase in the estimated mean of PM_{10} concentration. This means that, on average, the air pollution level, as represented by the PM_{10} index, tends to be higher in the period following the 35th observation compared to the preceding observations. This observation highlights the importance of monitoring and analyzing trends in PM_{10} concentration over time in order to understand the impact of external factors, such as pandemic-related measures on air pollution levels which is crucial for effective environmental management and public health.

Through the empirical example, we may suggest that the proposed robust estimation method seems to be able to effectively identify the change point in terms of its distribution, a task that the conventional individual control chart being not able to achieve in this specific dataset. It is noteworthy that while both charts presented in Fig. 1 and Fig. 2 identified the process shift at $i = 28$, there is a distinction in their ability to recognize the change point at $i = 35$. Specifically, the conventional individual control chart appears to overlook the shift at $i = 35$, whereas the proposed robust individual control chart successfully identifies it. This difference in detection may be attributed to the impact of inflated control limits influenced by a few outlying values, such as observations 28, 33 and 34. The primary factor is the distinctive construction of control limits based on specific charting procedures which leads to the recommendation of adopting the robust charting method in retrospective process analysis.

4.2 Simulation results for the existing and the proposed method

In this section, we aim to contrast the performance of various robust estimators for their corresponding efficiency in terms of the proportion of detected shifts. As displayed in Table 1, there are three types of robust estimators in estimating its means that were adopted in this comparison, specifically those based on Huber (*H*), Biweight (*B*), and Biweight with *M-Scale* (*BM*). The range of shift magnitudes under consideration spans from 0.5 to 3.0, and the sample sizes, denoted as *n,* vary from 10 to 80 observations.

Table 1. Proportion of Detected Shifts by Means of Huber (*H*), Biweight (*B*) and Biweight with *M-Scale* (*BM*) Estimators.

		Sample size n											
		10			20			40			80		
		H	*B*	*BM*	*H*	*B*	*BM*	*H*	*B*	*BM*	*H*	*B*	*BM*
Shift (Multiples of σ)	0.5	0.064	0.079	0.075	0.078	0.063	0.070	0.055	0.064	0.063	0.054	0.064	0.103
	1.0	0.184	0.174	0.196	0.212	0.211	0.223	0.173	0.196	0.246	0.200	0.218	0.276
	1.5	0.328	0.295	0.334	0.388	0.391	0.432	0.327	0.406	0.438	0.397	0.432	0.461
	2.0	0.491	0.499	0.512	0.581	0.593	0.620	0.573	0.606	0.618	0.570	0.604	0.623
	2.5	0.662	0.684	0.722	0.723	0.725	0.759	0.729	0.738	0.749	0.731	0.741	0.765
	3.0	0.765	0.778	0.796	0.819	0.830	0.844	0.807	0.836	0.844	0.824	0.843	0.855

The findings from this comparison indicate that the Biweight estimator (*B*) demonstrates better performance over the commonly employed Huber estimator (*H*), particularly as the sample size increases. Nevertheless, the Biweight integrating *M-Scale* estimator (*BM*) surpasses both the Huber and Biweight estimators, showcasing remarkable effectiveness, especially in adeptly addressing scenarios involving the shifts in mean.

In general, it is observed that the likelihood of detecting shifts tends to rise with an increase in both sample size and the magnitude of the shift. For example, when the sample size is varied from 10 to 80, and the magnitude of the shift is set to 3, the proportion of detected shifts increases for various estimators. Specifically, the *H* estimator shows an increase from 0.765 to 0.824, the *B* estimator from 0.778 to 0.843, and the *BM* estimator from 0.796 to 0.855. Additionally, when comparing the same sample size, it is worth noting that as the magnitude of the shift rises, the proportion of detected shifts also increases. Notably, the *BM* estimator appears to outperform the *H* and *B* estimators in this scenario. For instance, in the case of a sample size of 20 and a shift magnitude of 2.0, the proportions of detected shifts are 0.581 for *H*, 0.593 for *B*, and 0.620 for *BM* estimators respectively.

The Monte Carlo studies appear to confirm that the Biweight with *M-Scale* estimator excels in addressing out-of-control conditions as compared to other estimators, indicating its robustness and efficiency when data were shifted from its position, in which case all

estimators are inherently designed to be more sensitive to deviations from normality. These insights are further illustrated in Fig. 3.

Furthermore, it is evident from the study that as the magnitude of the shift increases, the proportion of detected shifts also increases. This means that the estimators are more effective in detecting larger changes in the data aligning with our purpose of identifying significant deviations from the expected behaviors.

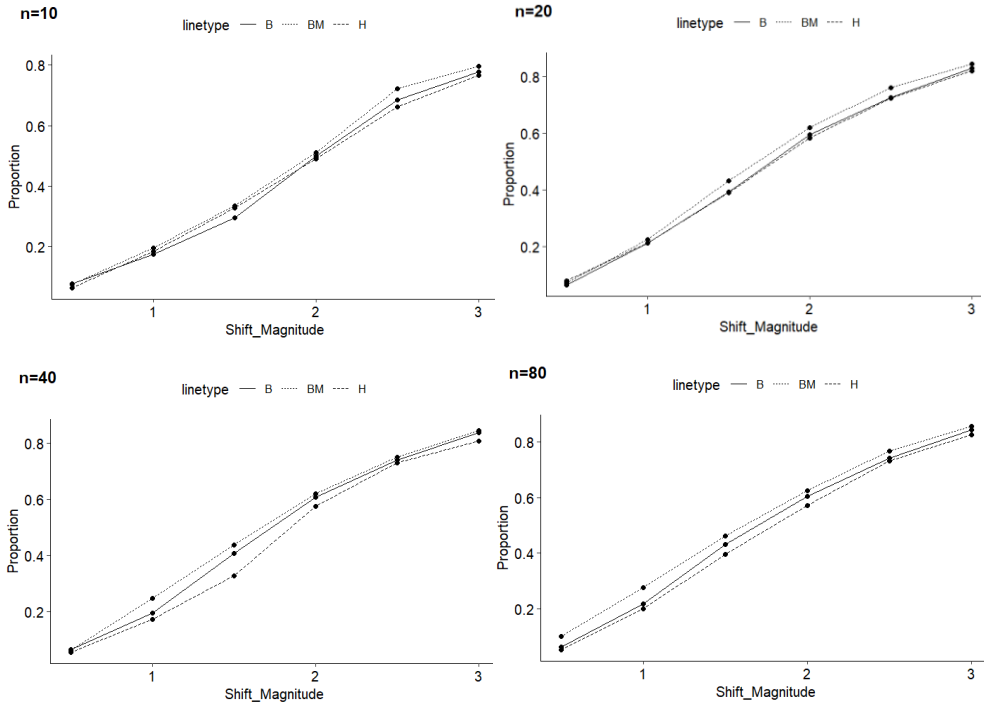

Fig. 3. Plots Depicting Proportion of Detected Shifts by Means of Huber (*H*), Biweight (*B*) and Biweight with *M-Scale* Estimators (*BM*)

5 Conclusion

In summary, robust control charts are a valuable tool in quality management and process control. They provide a means to monitor and maintain the stability and performance of processes in the face of various sources of variability and uncertainty.

In this study, our proposed robust procedure appears to outperform the conventional individual chart in real dataset application demonstrating their accuracy in detecting changes in the presence of outlying values conditions. In addition, through the adoption of robust charting procedure, the proposed method (Biweight with *M-Scale*) also tends to exhibit superior performance in comparison to those based on Huber and Biweight estimators. The results from the Monte Carlo studies by means of the proportions of detected shift suggest that the Biweight with *M-Scale* estimator stands out in effectively handling out-of-control conditions compared to other estimators. This indicates its robustness and efficiency, particularly when the data are shifted from their original positions. In such cases, all estimators are inherently designed to be more sensitive to deviations from normality.

While the proposed robust control charts offer significant advantages in quality management and process control, there are certain limitations and potential avenues for

further exploration. As for its limitation, the effectiveness of robust control charts might vary across different industries and processes. The suitability of these charts may depend on the nature of the data and the specific requirements of a given application. Thus, the implementation of comparative studies across different industries to assess the generalizability of the proposed robust control charts to understand how these charts perform in diverse contexts may provide valuable insights for further application. Nevertheless, it is also advisable to conduct more in-depth research on the proposed approach, encompassing aspects such as its application in scenarios involving multiple change points, variations in subgroup sample sizes and other pertinent factors to enhance its reliability.

References

1. D. C. Montgomery, *Introduction to Statistical Quality Control (6th ed.)*. Wiley (2005)
2. A. Yeganeh, S. C. Shongwe, PLoS ONE, **18(7)**, 1-26 (2023)
3. H. A. Wolfe, A. Taylor, R. Subramanyam, Paediatr. Anaesth, **31**(5), 539-547 (2021)
4. A. Reynolds, J. Mann, J. Cummings, N. Winter, E. Mete, L. Te Morenga, The Lancet, [online] **393**(10170), 434-445 (2019)
5. D. F. Andrews, P. J. Bickel et al., Princeton, N.J.: Princeton University Press (1972)
6. B. Iglewicz, D. C. Hoaglin, ASQC Quality Press (1993)
7. J. H. Sullivan, W. H. Woodall, J. Qual. Technol, **28**(3), 265-278 (1996)
8. D. A. Lax, JASA, **80**(391), 736-741 (1985)
9. L. G. Tatum, Technometrics, 127-141 (1997)
10. P. J. Huber, J. Wiley, New York (1981)
11. M. Abid, H. Z. Nazir, M. Riaz, Z. Lin, Trans. Inst. Meas. Control, **40**(13), 3860-3871 (2017)
12. M. O. A. Abu-Shawiesh, Journal of Mathematics and Statistics, **4**(2), 102-107 (2008)
13. A.P. Ariza Guerrero, R. Barreto Pombo, R. J. Herrera Acosta, J. Ind. Eng. Int., **15**(S1), 309-318 (2019)
14. V. J. Yohai, Ann. Stat., **15**(2), 642-656 (1987)
15. J. De Mast, K. C. B. Roes, Qual. Eng., **16**(3), 407-421 (2004)
16. Q. Peihua, Fl: Crc Press (2014)
17. R. Sheikhrabori, M. Aminnayeri, Commun. Stat. - Theory Methods, **51**(22), 7801-7818 (2021)
18. R. A. Maronna, R. Douglas Martin, V. J. Yohai, M. Salibián-Barrera, *Robust statistics: Theory and Methods (with R)*. John Wiley & Sons (2019)
19. J. Walach, P. Filzmoser, Š. Kouřil, D. Friedecký, T. Adam, J. Chemom, **34**(1) (2019)
20. K. S. Adekeye, J. A. Adewara, O. L. Aako, J. O. Olaomi, Qual. Reliab. Eng. Int., **37**(8), 3431-3440 (2021)
21. M. O. A. Abu-Shawiesh, IJQRM, **26**(5), 480-496 (2009)